KECK Geology Consortium
Learning Science Through Research
Published by Keck Geology Consortium
Short Contributions
30th Annual Symposium Volume
29th April, 2017
ISBN: 1528-7491

IMPLICATIONS OF PRE-CRETACEOUS MARBLES ALONG THE SUR FAULT ZONE, CALIFORNIA, USA: A STUDY OF CALCITE CRYSTALLOGRAPHIC PREFERRED ORIENTATIONS

ERICA A. WATTS, Mount Holyoke College
Research Advisor: Michelle Markley

INTRODUCTION

This study focuses on six samples of marble mylonites and fault rocks. The goals of this study are to assess the thermal and kinematic history of the Sur Fault using textures, specifically calcite crystallographic preferred orientations (CPOs). The study is in the Salinian Coast Ridge Belt (CRB). The CRB is a deep exposure of the Late Cretaceous California arc in the Santa Lucia Mountains (Chapman et al., 2014). The Sur Fault defines the boundary between the CRB and the Franciscan Complex (KJf). The KJf is comprised of late Mesozoic terrane of varied rocks that formed in an accretionary wedge in the western part of the Point Sur region (Hall, 1991). Here along the CRB, the Sur Fault zone juxtaposes marbles, Mesozoic and older felsic igneous rocks, and the KJf.

The Sur Fault Zone is currently a member of the dextral Neogene San Andreas Fault System, though the Franciscan-on-Coast Ridge Belt relationship present along the fault is thought to have been established in Late Cretaceous-early Cenozoic time (Dickinson, 1983; Dickinson et al., 2005; Jacobson et al., 2011). While the timing of early slip along the Sur Fault is well understood, the nature of the slip along the fault has been variously described in the literature as both a sinistral strike slip fault and/or a thrust fault (Dickinson, 1983; Hall, 1991; Dickinson et al., 2005; Chapman et al., 2016). In the field, we collected a suite of samples of pre-Cretaceous marbles along the Sur Fault Zone near Lucia, CA (Fig. 1 and Table 1).

METHODS

I present data from thin sections of the marble mylonite in the form of microstructural analysis and calcite crystallographic preferred orientations (CPOs). I cut thin sections from all six samples, including two sections from sample 16SLM2B, 2BI and 2BII, for petrographic microscope analysis. I analyzed deformation of the marble mylonite thin sections to quantify grain sizes, grain orientations and rock textures, while looking for kinematic indicators.

I polished the initial thin sections with colloidal silica and then added a carbon coating to prepare them for the Scanning Electron Microscope (SEM) using the Electron Backscatter Diffraction (EBSD) attachment. The EBSD is an attachment for the SEM that we used for the purpose of obtaining data, including, grain size, grain boundary, grain orientation, texture, phase identity and quantitative microstructural analysis. We gathered EBSD data at the University of Minnesota using the SEM-JEOL JSM-6500F Field Emission Scanning Electron Microscope at the Characterization Facility in the Department of Geology and Geophysics (Table 2). These data provided calcite grain CPO for microstructural analysis.

RESULTS

Sample Descriptions

16SLM2A and 16SLM2B

In hand sample, samples 2A and 2B are white and grey marbles with calcite grains on the scale of millimeters (mm) and smaller (Fig. 2 (a) and 2 (b)). Grey bands are mm-scale in width and defined by graphite. The white and grey bands are fine laminations, sometimes tightly and asymmetrically folded, and other times mantling centimeter (cm) scale porphyroclasts.

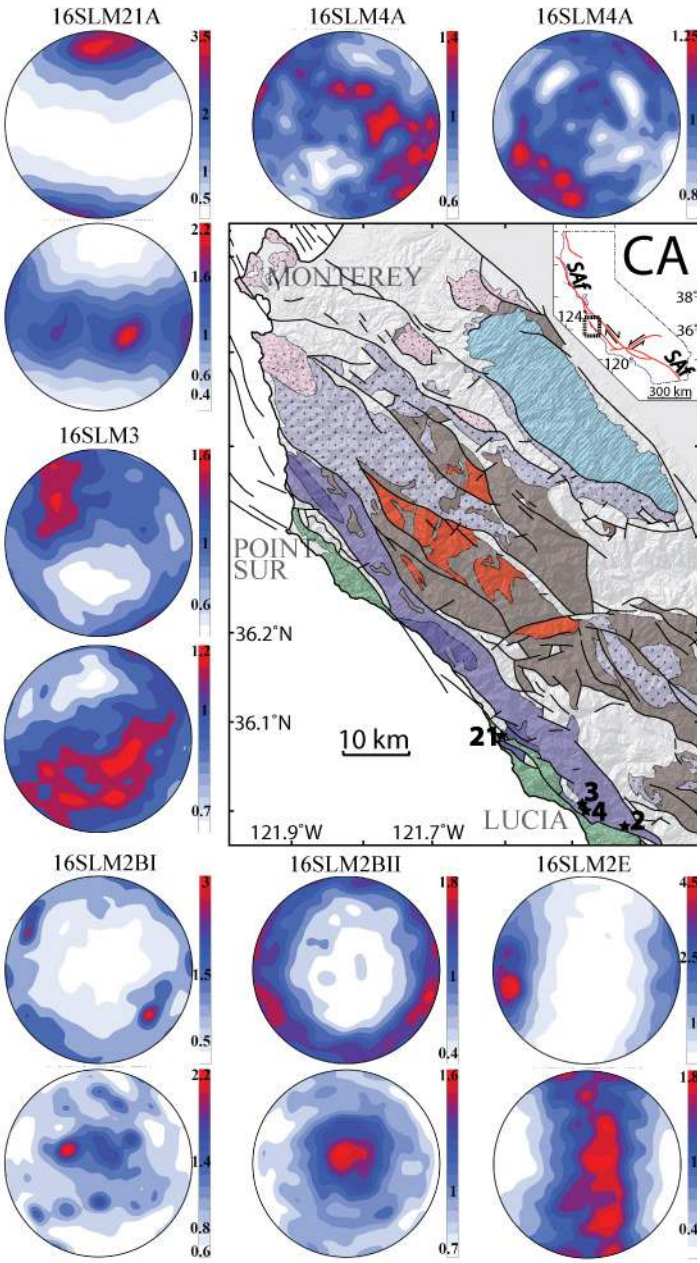

Figure 1. Regional and Geologic units map, and calcite CPO pole figures. The map exhibits locations from my study, denoted with a black star and the sample number. Sample locations 2, 3 and 4 are within the tonalitic to gabbroic orthogneiss and 21 is within the upper Cretaceous and younger sedimentary and alluvial deposits. The calcite CPO pole figures are arranged by sample name and location with the c-axis (0001) on top of the a-axis (2110). 16SLM4A calcite CPO c-axis (0001) is on the left and a-axis (2110) on the right. In the calcite CPO pole figures, the color red and the number associated with the color reveals it is that much stronger than the uniform distance. The color red is also showing the concentration of c-axis or a-axis oriented in that specific orientation.

Table 1.

Sample	UTM 10S	Latitude/Longitude
16SLM2	3983427 Northing	35°59'6.24" N
	0641242 Easting	121°25'59.60" W
16SLM3	3985138 Northing	36°0'4.63" N
	0635359 Easting	121°29'42.87" W
16SLM4A	3985550 Northing	36°0'18.13" N
	0635359 Easting	121°29'53.16" W
16SLM21A	3994707 Northing	36°5'20.14" N
	0625197 Easting	121°36'33.74" W

Table 1. Coordinates from the collected marble mylonite samples in my study.

Table 2.

Number of reflectors	75
Band edges	6 minimum
	8 maximum
Hough resolution	75
Binning	4x4
Milliseconds	18
Kv	25
Working distance (mm)	25
Probe current (nanoamps)	20
SEM mag	250
Match units	Calcite
Grain detection:	
Critical misorientation	10°
Allow boundary completion to	10°
Step sizes (microns):	
Marble coarse maps	25
Marble detail maps	1-2

Table 2. EBSD conditions using the JEOL JSM-6500F field emission SEM.

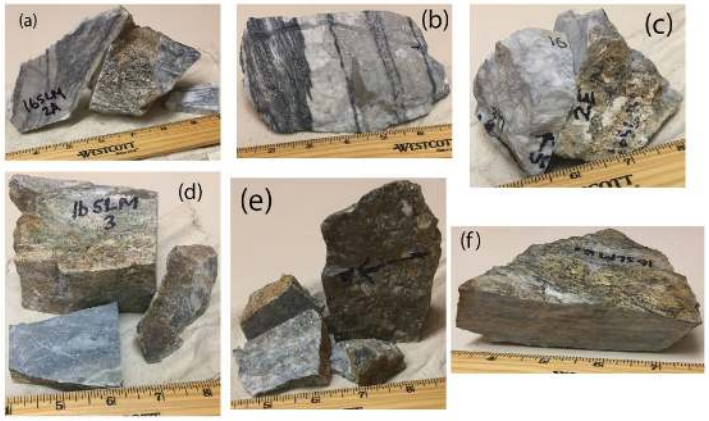

Figure 2. The collected hand samples in my study. 16SLM2A (a), 16SLM2B (b), 16SLM2E (c), 16SLM3 (d), 16SLM4A (e), and 16SLM21A (f).

There is no lineation apparent in the samples, and the laminations are likely the result of mylonitization. Thin mm-scale, delicate dolomite and calcite veins crosscut the lamination.

In thin section, calcite is the only major mineral. Minor minerals include phlogopite, chlorite, apatite, dolomite, titanite, tremolite or serpentine, and graphite. Calcite grains show polysynthetic twinning. The subrounded to subangular calcite grains range in size from 100-200 microns, and appear equant in the matrix. Calcite grain boundaries are serrate and many calcite grains contain either fluid or mineral inclusions that give them a cloudy character. Phlogopite is elongated and ranges in size from 10-100 microns. Chlorite is equant to elongate and ranges in size from 100-400 microns. Apatite grains are equant, rounded and ranging in size from 60-100 microns. Several veins are present and range in thickness from 60-100 microns.

16SLM2E

In hand sample, 2E is a grey and white marble (Fig. 2 (c)). Weathered faces are light and dark beige. The mineral composition is calcite, dolomite and muscovite. The sample appears brecciated; with dark and light grey veins running in multiple directions creating angular geometric patterns on the cm-scale.

In thin section, calcite is the major mineral and occurs most frequently. Trace minerals include dolomite, chlorite, phlogopite, apatite and titanite. There are multiple generations of calcite, revealed by granulated calcite grains with highly twinned and warped relic cores. Sections of calcite around the 'veins' exhibit newer generations of calcite. Calcite grains show lamellar and polysynthetic twinning. Subangular calcite appears equant to elongate with grains ranging in size from 60-200 microns. Calcite grain boundaries are serrate. Dolomite appears equant with grain sizes ranging from 60-400 microns. Dolomite grain boundaries appear wavy to serrate. Chlorite appears equant with grains ranging in size from 100-600 microns. Apatite grains are equant and approximately 115 microns in size. Chlorite, dolomite and calcite make up the composition of 'veins' that are approximately 200 microns thick. Clouded calcite is present with minute fluid inclusions. Clear foliation and lineation are absent in both hand sample and thin section.

16SLM3

In hand sample, 3 is a blueish dark grey marble (Fig. 2 (d)). Darker bands mantle centimeter-scale porphyroclasts. Banding is subvertical, and lineation dips steeply to the north. One clast exhibits an asymmetric shape in the plane parallel lineation, suggesting an east-side-up sense of shear. The marble has several white veins, ranging from 20-50 mm in length that cut across foliation. The sample is weathered exhibiting iron oxidation in some areas. It is coarse and dull in appearance.

In thin section, calcite is the major mineral and occurs most frequently. Minor minerals include apatite, biotite, quartz, 'Berlin blue' chlorite, dolomite and opaque minerals. Coarse calcite grain sizes vary and make up the majority of the matrix, revealing lamellar twinning. Individual calcite grains are subangular to subrounded without obvious crystallographic orientations of grains to reveal preferred orientation. Calcite grains are approximately 100 microns. There are striations within the equant calcite crystals; however, there are areas in thin section where the calcite experienced deformation showing elongate grain sizes. Calcite grain boundaries appear wavy to serrate. Apatite is elongated and ranges in grain size from 100-300 microns. 'Berlin blue' chlorite is elongated and ranges in grain size from 160-400 microns. The sample shows recrystallization of carbonate minerals in thin section.

16SLM4A

In hand sample, 4A is a dark grey marble breccia (Fig. 2 (e)). Most clasts are subangular and on the cm-scale and smaller, but one is decimeter-scale and appears to be a tonalite clast. The rounded breccia is composed mainly of calcite and ranges in size from 1-10 mm. The marble breccia has thin calcite veins that range in length, approximately 20-50 mm. The sample appears rusty and weathered even on freshly cut faces. A weak foliation is visible on one cut face of the sample. Otherwise, foliation and lineation are not apparent.

In thin section, calcite is the major mineral and occurs most frequently. Minor minerals include dolomite, muscovite, biotite, hornblende and chlorite. Calcite grains range in size from 60-200 microns and make up the fine-grained matrix. Calcite grains show lamellar twinning. Calcite grain boundaries are serrate. The calcite grains appear subangular. The grain boundaries surrounding biotite, hornblende and other trace minerals are wavy. Apatite grain sizes range from microns to mm in size. Quartz grain sizes range from 60-100 microns. There is a 100-micron thick vein comprised of the trace minerals with wavy grain boundaries in the calcite matrix.

16SLM21A

In hand sample, 21A is a light grey and beige marble with proto-mylonitic banding defined by stretched grains and grain aggregates (Fig. 2 (f)). Foliation dips shallow, 27° to the west, and the stretching lineation is close to down-dip. The proto-mylonite bands are approximately 3-60 mm in width. There are asymmetric porphyclasts and c'-type shear bands that show a reverse sense of shear.

In thin section, calcite is the major mineral with significant quartz and feldspar. Calcite grains appear equant and are very fine grained; they are too small to show twinning. The major minerals are 10s of microns in scale in the fine-grained matrix. Minor minerals include biotite, muscovite, hornblende and possibly dolomite. Calcite grains are subrounded to subangular. Biotite and hornblende grains appear subangular with serrate grain boundaries within the calcite matrix. Foliation and lineation are defined in thin section by elongate grain shapes, muscovite grains, and 100-micron wide ultramylonite shear zones. Porphyroclasts are made up of biotite, hornblende, calcite, feldspar, and possible dolomite and quartz. SC fabric is also present in thin section.

Calcite Crystallographic Preferred Orientations (CPOs)

Samples from site 2 show an intriguing range of textures and CPOs (Fig. 1). In hand samples, 2A and 2B are well-foliated white and grey marbles (Fig. 2). I did not collect EBSD data from sample 2A. Sample 2BI shows weak CPO (N = 5106 calcite grains) (Table 3). Calcite c-axes show a maximum but also a weak girdle, calcite a-axes show a weak maximum (about 90° from the c-axis maximum) and a poorly defined girdle (Fig. 1). Sample 2BII shows an extremely interesting and unusual CPO (N = 10629 calcite grains) (Table 3). C-axes define a strong girdle perpendicular to visible foliation, and a-axes show a strong maximum parallel to the foliation (subhorizontal) (Fig. 1).

It is possible that the CPOs of 2BI and 2BII are more similar than they appear. There are far fewer data from 2BI because of difficulty with the thin section, and so the CPO of 2BI is not as well constrained as those

Table 3.

Sample	16SLM2BI	16SLM2BII	16SLM2E	16SLM3	16SLM4A	16SLM21A
N	5106	10629	10354	12169	6416	13087
Calcite c-axis	{0001}	{0001}	{0001}	{0001}	{0001}	{0001}
PFJ	1.23	1.16	1.92	1.07	1.04	1.71
Max	3.24	1.84	4.83	1.65	1.44	3.65
Calcite a-axis	{2110}	{2110}	{2110}	{2110}	{2110}	{2110}
PFJ	1.07	1.04	1.22	1.02	1.01	1.18
Max	2.29	1.69	1.99	1.27	1.27	2.26

Table 3. Calcite CPO c-axis and a-axis pole figures. The EBSD performed stitch mapping to create calcite CPO pole figures. The EBSD also performed a detail map in order to assess variation within a single grain for deformation crystallization orientation. The EBSD counts each calcite grain one time (points per grain) and the N value is the total number of grains being counted on the calcite CPO pole figure with a maximum density value within a 6.5° radius (how many data points in that spot). The Max figure is the maximum density multiple of uniform distance. The PFJ value is the texture strength. The PFJ value measures the strength with the dependency of N, which is the maximum multiple distance, so the higher the N value, the higher the density resulting in a smaller value.

for many other samples. Another consideration is that 2BII has a more uniform grain size distribution in thin section than 2BI, and 2BII may be more uniformly and strongly formed.

From the same site, sample 2E shows a completely different texture in hand sample and CPO. C-axes define a very strong maximum (N = 10354), nearly orthogonal to a well-defined a-axis girdle (Fig. 1 and Table 3). The symmetry is slightly asymmetric. The strong CPO contrasts sharply with the appearance of the hand sample, which is dominated by grey veins and suggestive of brecciation (Fig. 1 and Fig. 2). It is likely that this texture developed later than the strong CPO.

The sample from site 3 shows evidence of both brittle and ductile deformation in thin section. The calcite CPO is weak even though the number of calcite grains measured (N = 12169) is relatively high (Table 3). C-axes show a weak maximum, and a-axes show a weak girdle nearly orthogonal to the c-axis maximum (Fig. 1).

The sample from site 4 also shows evidence of both brittle and ductile deformation in thin section. The calcite CPO is relatively weak, although in this case the weak CPO may be part reflect the relatively small number of calcite grains measured (N = 6416) (Table 3). Nonetheless, this sample's CPO is similar to the extremely unusual CPO displayed by sample 2BII (Fig. 1). For sample 4, the calcite c-axes define a girdle perpendicular to foliation and the sample's a-axes define a diffuse maximum parallel to foliation (Fig. 1).

Sample 21A is the only sample in this study that shows characteristics of a true mylonite, including reduced grain sizes, and a very strong foliation and lineation. Calcite c-axes (N = 13087) show a very strong maximum sub-perpendicular to foliation and lineation, with again a slight asymmetry (Fig. 1 and Table 3). Calcite a-axes define a girdle sub-parallel to foliation. Within this girdle, a-axes show three maxima at roughly even spacing, one of which is parallel to sample lineation (Fig. 1).

The sample CPO fabrics for calcite show some correlation with visible fabric. For example, 21A has a strong visible fabric in hand sample and a very strong CPO, whereas sample 4A has a weak CPO and fabric is absent in hand sample. However, the visible fabric and CPO correlation is inconsistent within the sample suite.

DISCUSSION

These rock textures and well-defined CPO fabrics indicate greenschist grade deformation. Although, calcite grains are able to produce a maximum around the Z-axis at low temperatures, <300°C (Passchier et al., 2005), sample 2B contains both calcite and graphite, which suggests a temperature range of 300-500°C (Dunn and Valley, 1992). Seaton et al. (2013), suggest marble has no crystallographic fabric at temperatures >500°C, likely reflecting a transition from dislocation creep to diffusion creep, so these samples likely deformed below this temperature. Many workers have used strength of CPO to assess relative temperature during deformation.

Seaton et al. (2013) also suggest shearing of calcite rods produce a very strong c-axis point maximum in the low temperature Barrovian domain, <400°C. Samples 2E and 21A reveal a strong c-axis point maximum in the CPOs, perhaps suggestive of a lower relative temperature than 3 and 4A. From these considerations, I infer peak temperatures during deformation between 300-400°C for this sample suite.

The EBSD data reveal atypical a-axis maxima in samples 2BII and 4A, and it is likely that no one has reported this atypical CPO in calcite before in the literature. However, Sullivan and Beane (2010) report these fabrics for quartzites that have clearly experienced constrictional deformation, confirming constrictional quartz a-axis patterns for the first time and proposing that a-axis maxima may be characteristic of quartz in L-tectonites. Because quartz and calcite are both hexagonal minerals, this interpretation may be useful for my samples. However, neither sample appears to be an L-tectonite or shows any evidence of constrictional strain. Sullivan and Beane (2010) confirm natural fabrics produced under apparent constrictional strain are rare in literature, and constrictional deformation of rocks has yet to be reported experimentally. Other possible interpretations of this unusual CPO are inheritance from the protolith.

In this region, marble is the oldest material and calcite grains reveal evidence for multiple generations of deformation, making these textures even more difficult to interpret.

The remaining samples show calcite CPOs of varying strengths, but all with a c-axis maximum and sub-perpendicular a-axis girdle. Sample 21A is a well-defined example with strong foliation and lineation, revealing asymmetry of c-axis max with regard to foliation, and lineation indicates non-coaxial deformation. We interpret the fabrics of the other samples (2E and 3) also as the result of non-coaxial deformation associated with shearing on the Sur Fault. Unfortunately, most samples show no lineation, and most thin sections are only tentatively oriented with respect to foliation, so I am not able to infer the geometry of slip on the Sur Fault from this sample suite. The exception is sample 21A, which shows evidence for oblique slip with both dextral and reverse components.

CONCLUSIONS

In the region, marble is the oldest lithology, and it is much less competent than the granitoids or Franciscan complex lithologies. Marble here is also poly-metamorphic, and this complex history confounds a clear interpretation of the marble mylonite rock suite. The samples are from a mapped mylonite zone, but not all of the collected samples are mylonites, some appear brecciated and others merely foliated. The deformation histories are non-coaxial (with the exception of 2B and 4A), but probably experienced multiple deformation phases at temperatures between 300°C and 400°C. Sample 2BII has a pronounced a-axis max suggesting constriction deformation. Constriction (pure triaxial strain) may have produced the CPOs, but this interpretation is extremely tentative.

ACKNOWLEDGMENTS

I would like to thank the KECK Consortium, ExxonMobil and the National Science Foundation for affording the opportunity to conduct research, Dr. Sarah Jo Brownlee, Wayne State University for her knowledge of EBSD data and assistance with my project, overall, and Dr. Alan Chapman, Macalester College for his support. I would like to thank Michelle Markley at Mount Holyoke College for her guidance, support and encouragement.

REFERENCES CITED

Chapman, A. D., Ducea, M. N., Kidder, S., & Petrescu, L. (2014). Geochemical constraints on the petrogenesis of the Salinian arc, central California: Implications for the origin of intermediate magmas. *Lithos*, *200*, 126-141.

Chapman, A.D., Jacobson, C.E., Ernst, W.G., Grove, M., Dumitru, T., Hourigan, J., and Ducea, M., 2016, Assembling the world's type shallow subduction complex: Detrital zircon geochronologic constraints on the origin of the Nacimiento block, central California Coast Ranges: Geosphere, v. 12, p. 533–557. doi:10.1130/GES01257.1

Dickinson, W.R., 1983, Cretaceous sinistral strike slip along the Nacimiento fault in coastal California: American Association of Petroleum Geologists Bulletin, v. 67, p. 624–645.

Dickinson, W.R., Ducea, M., Rosenberg, L.I., Greene, H.G., Graham, S.A., Clark, J.C., Weber, G.E., Kidder, S., Ernst, W.G., and Brabb, E.E., 2005, Net dextral slip, Neogene San Gregorio–Hosgri fault zone, coastal California: Geologic evidence and tectonic implications: Geologi cal Society of America Special Paper 391, 43 p., doi:10.1130/2005.2391.

Dunn, S.R., and Valley, J.W. (1992). Calcite-graphite isotope thermometry: a test for polymetamorphism in marble, Tudor gabbro aureole, Ontario, Canada. Journal of Metamorphic Geology, 10(4), 487-501. DOI: 10.1111/j.1525-1314.1992.tb00100.x

Hall, C.A., Jr., 1991, Geology of the Point Sur–Lopez Point region, Coast Ranges, California: A part of the Southern California allochthon: Geological Society of America Special Paper 266, 44.

Jacobson, C.E., Grove, M., Pedrick, J.N., Barth, A.P., Marsaglia, K.M., Gehrels, G.E., and Nourse, J.A., 2011, Late Cretaceous–early Cenozoic evolution of the southern California margin in ferred from provenance of trench and forearc sediments: Geological Society of America Bulletin, v. 123, no. 3–4, p. 485–506.

Passchier, C.W., and Trouw, R. A.J. (2005). Microtectonics (2nd ed.). Berlin: Springer.

Seaton, N. C.A., Teyssier, C., Whitney, D.L., and Heizler, M.T. (2013). Quartz and calcite microfabric transitions in a pressure and temperature gradient, Sivrihisar, Turkey. Geodinamica Acta, 26:3-4, 191-206, DOI: 10.1080/09853111.2013.858952

Sullivan, W.A., and Beane R.J. (2010). Asymmetrical quartz crystallographic fabrics formed during constrictional deformation. Journal of Structural Geology, 32(10), 1430-1443.